Sigma Journal of Engineering and Natural Sciences
Web page info: https://sigma.yildiz.edu.tr
DOI: 10.14744/sigma.2023.00139

Research Article

3D FEM analysis of stress concentrations in a rectangular thick plate with PZT inclusions under bending

Ülkü BABUŞCU YEŞİL[1,*], Fatih AYLIKÇI[1]

[1]*Department of Mathematical Engineering, Yildiz Technical University, Istanbul, 34220, Türkiye*

ARTICLE INFO

Article history
Received: 22 October 2021
Revised: 25 December 2021
Accepted: 06 February 2022

Keywords:
Piezoelectric Inclusions; Stress Concentration; 3D Finite Elements Method

ABSTRACT

The present study is a prior attempt to study the influence of the PZT inclusion(s) in the rectangular elastic plate under bending on the stress concentration of this plate utilizing 3D exact equations of the elasto- and piezo-elastostatics theories. The corresponding boundary-value problem is formulated within the scope of the three dimensional exact equations of electro-elasticity theory using the piecewise-homogeneous body model and is solved numerically by the three dimensional Finite Element Method. It is assumed that the plate has simply-supported mechanically and short-circuit conditions with respect to the electric potential along all its lateral edge surfaces and ideal contact conditions are provided at the interface surfaces between the PZT inclusion(s) and the elastic matrix. All algorithms and programs required for the numerical solution are made by the authors. The effects of various matrix materials, the size, volume fraction and location of the piezoelectric inclusion as well as the coupling effect between the mechanical and electrical fields, in addition to the effects of interaction between the neighboring PZT inclusions in a simply-supported rectangular thick plate under bending force on the stress distributions therein are investigated and discussed. It is established that PZT inclusion(s) within the rectangular plate under bending force causes a decrease in the values of normal stresses and causes an increase in the values of shear stresses at the interface between the matrix and PZT inclusion(s).

Cite this article as: Babuşcu Yeşil Ü, Aylıkçı F. 3D FEM analysis of stress concentrations in a rectangular thick plate with PZT inclusions under bending. Sigma J Eng Nat Sci 2023;41(6):1197–1208.

INTRODUCTION

The piezoelectric property is a property seen in some materials without central symmetry in their crystalline internal structure. When an external force is applied to these materials, that is, when the material changes shape, polarization occurs in its structure. In other words, there is a situation that can create an electric current in the structure (direct effect). Conversely, when the material is placed in an electric field, mechanical deformation occurs in its structure (indirect effect). These effects are related to the change in polarization density inside the material. The response of piezoelectric materials to mechanical action depends on the crystal orientation determined by the arrangement of atoms in the crystal structures and the angular values between the

***Corresponding author.**
*E-mail address: ubabuscu@yildiz.edu.tr

This paper was recommended for publication in revised form by Regional Editor Ahmet Selim Dalkilic

applied mechanical stress and the direction of the elongation [1]. The dual properties of piezoelectric materials are utilized in many advanced technological applications such as actuators, sensors, transducers and generators. Recently, piezoelectric materials, which have a wide research area, have generally been used by combining (integrating) them with non-piezoelectric materials. There are many studies in the literature on piezoelectric materials containing discontinuities in various geometric forms.

Wang [2] develop a solution for an infinite, piezoelectric medium containing a piezoelectric, ellipsoidal inclusion by using Green's function technique. A piezoelectric ellipsoidal inhomogeneity embedded in a non-piezoelectric elastic matrix was analyzed via equivalent inclusion method by Fan and Qin [3]. Xu and Rajapakse [4] considered coupled elastic and electric fields in piezoelectric solids with arbitrary shaped defects (cavities, inclusions, cracks, etc.) under the assumptions of plane strain or stress conditions by a boundary integral equation based on closed form Green's functions. Effect of cracks on structures were studied by using finite element method by Gonenli, Das and Ozturk [5,6,7]. Xiao and Bai [8] investigated stress analysis for a circular piezoelectric fiber sensor embedded in a non-piezoelectric elastic material based on Eshelby's equivalent inclusion method.

Spherically symmetric deformation of an inclusion-matrix problem, which consists of an infinite isotropic matrix and a spherically uniform anisotropic piezoelectric inclusion was studied in [9]. Mishra et al. [10] analyzed an elliptical piezoelectric inclusion embedded in an infinite piezoelectric matrix in the framework of linear piezoelectricity by using the conformal mapping technique in [10] and in the framework of antiplane piezoelectricity in [11]. The piezoelectricity problems containing arbitrary elliptical inhomogeneities in an infinite medium was studied by Lee et al. [12]. The Green's function for an infinite piezoelectric medium with an elliptic hole filled with air or without air under the generalized line dislocation and the generalized line force was given by Zhou et al. [13]. They discussed the interaction of an arbitrary distributed small crack and an elliptic hole in plane piezoelectric medium subjected to uniform electro-mechanical loads at infinity. Yang and Gao [14] addressed the plane problems of multiple piezoelectric circular inclusions in a non-piezoelectric matrix based on the complex potentials. The problem of the stress state in an orthotropic piezoelectric body with a triaxial ellipsoidal inclusion under homogeneous force and electric loads was studied by Kirilyuk and Levchuk [15]. The problem was solved by the Eshelby method of equivalent inclusion generalized to the case of a piezoelectric orthotropic space. In [16], the electrostatic analysis of a thick plate containing a prismatic inclusion made of piezoelectric material under the effect of axial tensile force was investigated. In summary, the aforementioned works focused on problems involving piezoelectric inclusion(s) and sensors in various forms for infinite media or plane problems.

In this study, a mathematical model for the three-dimensional stress analysis of rectangular plates under the effect of bending and containing rectangular prismatic inclusion(s) made of piezoelectric material, is presented with the help of the piecewise homogeneous body model and the 3D exact equations of the electro-elasticity theory, which are numerically examined using the three-dimensional finite element method. Using the mathematical model presented, the effect of the size, location of the piezoelectric inclusion/inclusions and volume fraction as well as the coupling effect between the electrical and mechanical fields on the static analysis of the rectangular plate are studied.

Theory

It is assumed that the rectangular prismatic inclusion(s) in the structure are located along the posterior thickness of the plate (Ox_3 axis) and are parallel to the Ox_3 coordinate axis (Figure 1).

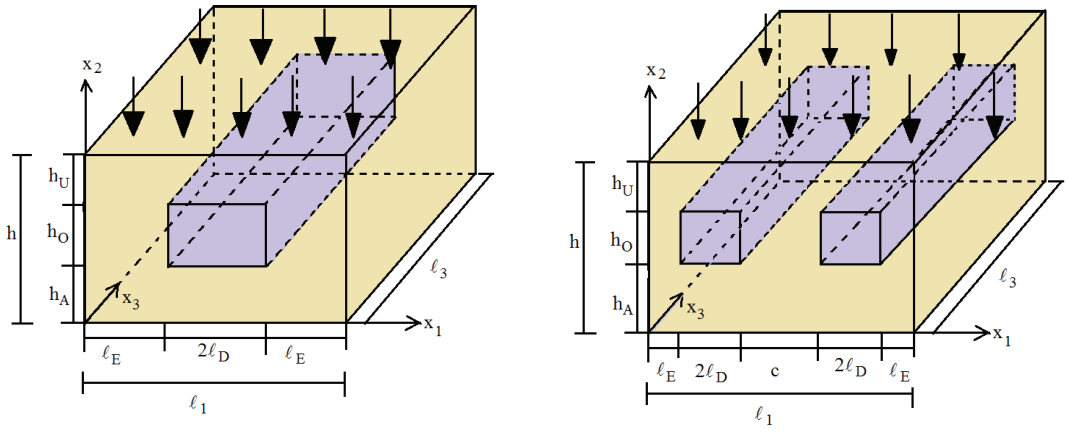

Figure 1. The geometry and loading of (a) plate containing a single PZT inclusion (Problem 1) b) plate containing double PZT inclusions (Problem 2).

The solution region of the problems discussed are:
For Problem 1:

$$\begin{aligned}&\Omega=\Omega'\cup\Omega_I=\left\{\,0\le x_1\le \ell_1, 0\le x_2\le h\,, 0\le x_3\le \ell_3\right\}\\&\Omega_I=\left\{\,\ell_E\le x_1\le \ell_1-\ell_E, h_A\le x_2\le h_A+h_O\,, 0\le x_3\le \ell_3\right\}\\&\Omega'=\Omega/\Omega_I\end{aligned}\tag{1}$$

For Problem 2:

$$\begin{aligned}&\Omega=\Omega''\cup\Omega_I\cup\Omega_{II}=\left\{\,0\le x_1\le \ell_1, 0\le x_2\le h\,, 0\le x_3\le \ell_3\right\}\\&\Omega_I=\left\{\,\ell_E\le x_1\le \ell_1-\ell_E, h_A\le x_2\le h_A+h_O\,, 0\le x_3\le \ell_3\right\}\\&\Omega_{II}=\left\{\,\ell_E+2\ell_D+c\le x_1\le \ell_1-\ell_E, h_A\le x_2\le h_A+h_O\,, 0\le x_3\le \ell_3\right\}\\&\Omega''=\Omega/\left(\Omega_I\cup\Omega_{II}\right)\end{aligned}\tag{2}$$

Here, for Problem 1 (Problem 2), Ω_I (Ω_I and Ω_{II}) shows the region where the inclusion(s) are located, and Ω' or Ω'' shows the region outside the inclusion(s) (matrix). The plate is simply supported on all its lateral surfaces, that the electrical potential is zero, and that it is subject to a uniformly distributed pressure force only from its upper surface. In addition, it is assumed that no mechanical and/or electrical loads act on the lateral surfaces of the plate or the inclusion and matrix interfaces. It is accepted that ideal contact conditions are provided at the interface between the inclusion contained in the plate and the matrix, and that the PZT inclusion is grounded from all surfaces (ie, there is no electrical displacement change in the normal direction). It should be noted that the mathematical modeling will be given by assuming that the material of both the inclusion and the surrounding region (matrix) is a piezoelectric material in order to be more general. However, in numerical calculations, the case where the matrix material is an elastic material will be taken into account. In mathematical modeling, the superscript (1) will be used to represent the dimensions of the matrix material and the superscript (2) and (3) will be used for the inclusion material.

Accordingly, the equilibrium equations provided in the solution region are:

$$\frac{\partial T_{ji}^{(m)}}{\partial x_j}=0,\frac{\partial D_j^{(m)}}{\partial x_j}=0\tag{3}$$

The electro-mechanical relations are:

$$\begin{aligned}&T_{ij}^{(m)}=c_{ijkl}^{(m)}s_{kl}^{(m)}-e_{kij}^{(m)}E_k^{(m)},\;\; D_i^{(m)}=e_{ikl}^{(m)}s_{kl}^{(m)}+\varepsilon_{ik}^{(m)}E_k^{(m)}\\&s_{kl}^{(m)}=\frac{1}{2}\left(\frac{\partial u_k^{(m)}}{\partial x_l}+\frac{\partial u_l^{(m)}}{\partial x_k}\right),\;\; E_k^{(m)}=-\frac{\partial\phi^{(m)}}{\partial x_k}\;\;,i;j;k;l=1,2,3\end{aligned}\tag{4}$$

In Eqs. (3) and (4), when there is a single (double) inclusion in the structure, the parameter m takes the values m=1,2 (m=1,2,3) and all quantities referring to the matrix (inclusion) material will be marked by the superscript 1 (2 and 3) and the following notation is used: $T_{ij}^{(m)}$ is the stress tensor component, $s_{kl}^{(m)}$ is the Green strain tensor component, $u_i^{(m)}$ is the displacement vector's component, $D_i^{(m)}$ is the electrical displacement vector's component, $E_k^{(m)}$ is the electrical field vector's component, $\phi^{(m)}$ is the electric potential, $e_{kij}^{(m)}$ is the piezoelectric constant, $\varepsilon_{ik}^{(m)}$ is the dielectric (permittivity) constant, and $c_{ijkl}^{(m)}$ is the component of elastic stiffness matrix. Compact matrix notation is used to write constitutive equations in matrix form. This notation reduces the pairs of indices *ij* or *kl* to a single index such as *p* or *q* as follows:

$$\begin{aligned}&c_{ijkl}\to c_{pq},\;\; e_{ikl}\to e_{ip},\;\; T_{ij}\to T_p\\&11\to 1,\;\; 22\to 2,\;\; 33\to 3,\;\; 23\;(32)\to 4,\;\; 31\;(13)\to 5,\;\; 12\;(21)\to 6\end{aligned}$$

If the constitutive equations of the material are arranged according to the new index notation:

$$T_p^{(m)}=c_{pq}^{(m)}s_q^{(m)}-e_{kp}^{(m)}E_k^{(m)},D_i^{(m)}=e_{iq}^{(m)}s_q^{(m)}+\varepsilon_{ik}^{(m)}E_k^{(m)}\tag{5}$$

or in matrix form:

$$\begin{Bmatrix}T_1^{(m)}\\T_2^{(m)}\\T_3^{(m)}\\T_4^{(m)}\\T_5^{(m)}\\T_6^{(m)}\end{Bmatrix}=\begin{Bmatrix}c_{11}^{(m)}&c_{12}^{(m)}&c_{13}^{(m)}&c_{14}^{(m)}&c_{15}^{(m)}&c_{16}^{(m)}\\c_{21}^{(m)}&c_{22}^{(m)}&c_{23}^{(m)}&c_{24}^{(m)}&c_{25}^{(m)}&c_{26}^{(m)}\\c_{31}^{(m)}&c_{32}^{(m)}&c_{33}^{(m)}&c_{34}^{(m)}&c_{35}^{(m)}&c_{36}^{(m)}\\c_{41}^{(m)}&c_{42}^{(m)}&c_{43}^{(m)}&c_{44}^{(m)}&c_{45}^{(m)}&c_{46}^{(m)}\\c_{51}^{(m)}&c_{52}^{(m)}&c_{53}^{(m)}&c_{54}^{(m)}&c_{55}^{(m)}&c_{56}^{(m)}\\c_{61}^{(m)}&c_{62}^{(m)}&c_{63}^{(m)}&c_{64}^{(m)}&c_{65}^{(m)}&c_{66}^{(m)}\end{Bmatrix}\begin{Bmatrix}s_1^{(m)}\\s_2^{(m)}\\s_3^{(m)}\\s_4^{(m)}\\s_5^{(m)}\\s_6^{(m)}\end{Bmatrix}-\begin{Bmatrix}e_{11}^{(m)}&e_{21}^{(m)}&e_{31}^{(m)}\\e_{12}^{(m)}&e_{22}^{(m)}&e_{32}^{(m)}\\e_{13}^{(m)}&e_{23}^{(m)}&e_{33}^{(m)}\\e_{14}^{(m)}&e_{24}^{(m)}&e_{34}^{(m)}\\e_{15}^{(m)}&e_{25}^{(m)}&e_{35}^{(m)}\\e_{16}^{(m)}&e_{26}^{(m)}&e_{36}^{(m)}\end{Bmatrix}\begin{Bmatrix}E_1^{(m)}\\E_2^{(m)}\\E_3^{(m)}\end{Bmatrix}$$

$$\begin{Bmatrix}D_1^{(m)}\\D_2^{(m)}\\D_3^{(m)}\end{Bmatrix}=\begin{Bmatrix}e_{11}^{(m)}&e_{12}^{(m)}&e_{13}^{(m)}&e_{14}^{(m)}&e_{15}^{(m)}&e_{16}^{(m)}\\e_{21}^{(m)}&e_{22}^{(m)}&e_{23}^{(m)}&e_{24}^{(m)}&e_{25}^{(m)}&e_{26}^{(m)}\\e_{31}^{(m)}&e_{32}^{(m)}&e_{33}^{(m)}&e_{34}^{(m)}&e_{35}^{(m)}&e_{36}^{(m)}\end{Bmatrix}\begin{Bmatrix}s_1^{(m)}\\s_2^{(m)}\\s_3^{(m)}\\s_4^{(m)}\\s_5^{(m)}\\s_6^{(m)}\end{Bmatrix}+\begin{Bmatrix}\varepsilon_{11}^{(m)}&\varepsilon_{12}^{(m)}&\varepsilon_{13}^{(m)}\\\varepsilon_{21}^{(m)}&\varepsilon_{22}^{(m)}&\varepsilon_{23}^{(m)}\\\varepsilon_{31}^{(m)}&\varepsilon_{32}^{(m)}&\varepsilon_{33}^{(m)}\end{Bmatrix}\begin{Bmatrix}E_1^{(m)}\\E_2^{(m)}\\E_3^{(m)}\end{Bmatrix}\tag{6}$$

the following boundary conditions are satisfied on all the lateral surfaces:

$$\begin{aligned}&u_2^{(m)}\big|_{x_1=0;\ell_1}=u_2^{(m)}\big|_{x_3=0;\ell_3}=0,\\&\phi^{(m)}\big|_{x_1=0;\ell_1}=\phi^{(m)}\big|_{x_3=0;\ell_3}=0,\\&T_{11}^{(m)}\big|_{x_1=0;\ell_1}=T_{13}^{(m)}\big|_{x_1=0;\ell_1}=0\\&T_{31}^{(m)}\big|_{x_1=0;\ell_3}=T_{33}^{(m)}\big|_{x_1=0;\ell_3}=0\\&T_{22}^{(m)}\big|_{x_2=h}=p,\\&T_{2i}^{(m)}\big|_{x_2=0}=T_{21}^{(m)}\big|_{x_2=h}=T_{23}^{(m)}\big|_{x_2=h}=0\end{aligned}\tag{7}$$

and the following contact conditions at the interfaces are satisfied:

$$\begin{aligned}&u_i^{(1)}n_i^{(1)}\big|_S=u_i^{(k)}n_i^{(k)}\big|_S,\\&T_{ij}^{(1)}n_j^{(1)}\big|_S=T_{ij}^{(k)}n_j^{(k)}\big|_S,\\&\phi^{(1)}n^{(1)}\big|_S=\phi^{(k)}n^{(k)}\big|_S,\\&D_i^{(1)}n_i^{(1)}\big|_S=D_i^{(k)}n_i^{(k)}\big|_S\end{aligned}\tag{8}$$

In Eq. (8), k=2 (k=2,3) for Problem 1 (Problem 2). $n_j^{(s)}$ (k=1,2,3) is the component of the unit outward normal

vector of surface S, and S represents the surface of the inclusions and is equal to Eq. (9) for Problem 1, and Eq. (10) for Problem 2.

$$\begin{aligned} S = &\left\{(x_1,x_2,x_3)\middle| x_1=\ell_E,\ h_A\le x_2\le h_A+h_O,\ 0\le x_3\le \ell_3\right\}\cup \\ &\left\{(x_1,x_2,x_3)\middle| x_1=\ell-\ell_E,\ h_A\le x_2\le h_A+h_O,\ 0\le x_3\le \ell_3\right\}\cup \\ &\left\{(x_1,x_2,x_3)\middle| \ell_E\le x_1\le \ell-\ell_E,\ x_2=h_A,\ 0\le x_3\le \ell_3\right\}\cup \\ &\left\{(x_1,x_2,x_3)\middle| \ell_E\le x_1\le \ell-\ell_E,\ x_2=h_A+h_O,\ 0\le x_3\le \ell_3\right\} \end{aligned} \tag{9}$$

$$\begin{aligned} S = &\left\{(x_1,x_2,x_3)\middle| x_1=\ell_E,\ h_A\le x_2\le h_A+h_O,\ 0\le x_3\le \ell_3\right\}\cup \\ &\left\{(x_1,x_2,x_3)\middle| x_1=\ell_E+2\ell_D,\ h_A\le x_2\le h_A+h_O,\ 0\le x_3\le \ell_3\right\}\cup \\ &\left\{(x_1,x_2,x_3)\middle| \ell_E\le x_1\le \ell_E+2\ell_D,\ x_2=h_A,\ 0\le x_3\le \ell_3\right\}\cup \\ &\left\{(x_1,x_2,x_3)\middle| \ell_E\le x_1\le \ell_E+2\ell_D,\ x_2=h_A+h_O,\ 0\le x_3\le \ell_3\right\} \\ &\left\{(x_1,x_2,x_3)\middle| x_1=\ell_1-(\ell_E+2\ell_D),\ h_A\le x_2\le h_A+h_O,\ 0\le x_3\le \ell_3\right\}\cup \\ &\left\{(x_1,x_2,x_3)\middle| x_1=\ell_1-\ell_E,\ h_A\le x_2\le h_A+h_O,\ 0\le x_3\le \ell_3\right\}\cup \\ &\left\{(x_1,x_2,x_3)\middle| \ell_1-(\ell_E+2\ell_D)\le x_1\le \ell_1-\ell_E,\ x_2=h_A,\ 0\le x_3\le \ell_3\right\}\cup \\ &\left\{(x_1,x_2,x_3)\middle| \ell_1-(\ell_E+2\ell_D)\le x_1\le \ell_1-\ell_E,\ x_2=h_A+h_O,\ 0\le x_3\le \ell_3\right\} \end{aligned} \tag{10}$$

The boundary value problem is solved numerically with the help of three-dimensional (3D) finite element modeling. The solution of the problems discussed was made for the half (1/2) region by making use of the symmetry of the structural element and the loading with respect to $x_1/\ell_1 = 1/2$. The solution region is discretized into 8-node rectangular prismatic finite elements separately for the matrix and the inclusion material in accordance with the geometry (Figure 2). The electrical potential (φ) and the displacements in the direction of the three axes are taken as unknowns in the nodes.

Shape functions, defined by the product of linear Lagrangian interpolations, are used at the nodes of the rectangular prismatic sample element (Figure 2) [17]. Displacement and electrical potential functions in each finite element within the framework of the finite element method

$$\begin{Bmatrix} u_i^{(e)} \\ \phi^{(e)} \end{Bmatrix} = \sum_{k=1}^{8} \begin{Bmatrix} u_{ik}^{(e)} \\ \phi_k^{(e)} \end{Bmatrix} N_k \tag{11}$$

are represented in serial form. For FEM modeling of the boundary value problem, the functional that expresses the total electro-mechanical energy accumulated in the structure

$$\begin{aligned} \Pi(u_1,u_2,u_3,\phi) = &\sum_{m=1}^{2}\iiint_{\Omega_m}\left[\frac{1}{2}G_{ijkl}^{(m)}\frac{\partial u_i^{(m)}}{\partial x_j}\frac{\partial u_k^{(m)}}{\partial x_l}+R_{ijk}^{(m)}\frac{\partial\phi^{(m)}}{\partial x_i}\frac{\partial u_j^{(m)}}{\partial x_k}-\frac{1}{2}\varepsilon_{ij}^{(m)}\frac{\partial\phi^{(m)}}{\partial x_k}\frac{\partial\phi^{(m)}}{\partial x_l}\right]d\Omega_m \\ &-\int_0^{\ell_3}\int_0^{\ell_1} p\,u_2^{(1)}\Big|_{x_2=h}dx_1dx_3-\int_0^{\ell_3}\int_0^{\ell_1} D_1^{(1)}\phi^{(1)}\Big|_{x_2=0;h}dx_1dx_3 \end{aligned} \tag{12}$$

is used [18]. The solution of the boundary value problem handled with the help of the Π functional, Eq. (11) expressions, and the known Ritz technique is reduced to the solution of

$$\mathbf{Ku} = \mathbf{F} \tag{13}$$

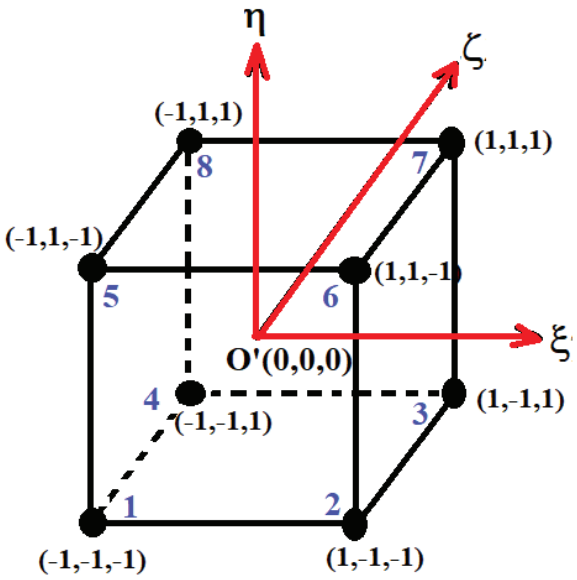

Figure 2. Rectangular prismatic sample element, position of nodes and coordinates of nodes

linear algebraic equation system. In Eq. (13), **K** is the coefficient (Stiffness) matrix, **u** is the vector containing the unknowns, and **F** is the right-hand side (force) vector. The reduced system is found by applying the displacements to the system of Eqs. (13) and the boundary conditions according to the electric potential given in Eq. (7). With the solution of the reduced system, the sought quantities in the nodes are obtained and the stress distributions in the structure are determined with the help of the constitutive equations given in Eq. (6). It will be attempted to determine the mutual effects of various geometric and material parameters and electrical and mechanical fields on these stress distributions.

RESULTS AND DISCUSSION

In solving the boundary value problems with the help of the finite element method, it is assumed that the inclusion material consists of piezoelectric (PZT) material, and the matrix material surrounding the inclusion consists of elastic material. Since the considered problem is symmetric about the $x_1 = \ell_1/2$ plane, only half of the region is used. For the FEM modeling, 6400 rectangular prismatic finite elements, 7497 nodes and 27591 NDOFs are used in total. First, for testing the mesh sensitivity, Figure 3 is given. The parameter N, M and NZ shows the number of rectangular FEs along the Ox_1 axis, Ox_2 axis and Ox_3 axis, respectively. Figs. 3(a-c) show the influence of (a) N, (b) M and (c) NZ on the values of σ_{11}/p for the case $E_2/E_1 = 1$ and $h/\ell_1 = 0.10$ in the cross section of $x_3 = \ell_3/2,\ x_2 = 0$. It follows from the graphs that the values of σ_{11}/p approach a certain limit value by increasing the parameters. These

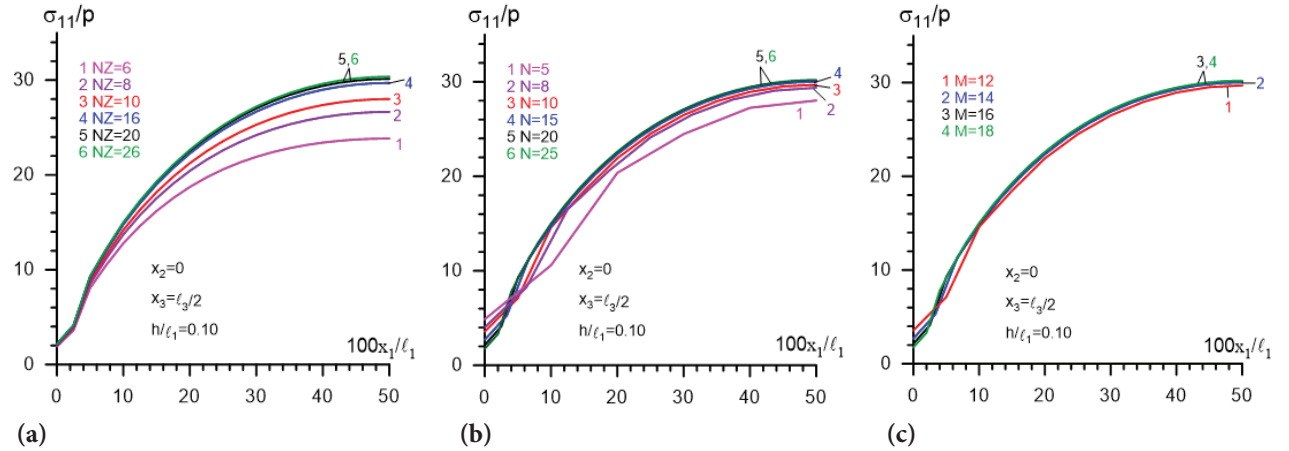

Figure 3. Influence of the number of rectangular FEs along the (a) Ox_3 axis i.e. NZ, (b) Ox_1 axis i.e. N and (c) Ox_2 axis i.e. M on the values of σ_{11}/p for the case $(E_2/E_1=1)$ and $h/\ell_1=0.10$ in the cross section of $x_3=\ell_3/2,\ x_2=0$.

Table 1. Material parameters of the PZT-5H materials $C_{ij}\left(10^{10}\,N/m^2\right), e_{ij}\left(C/m^2\right), \varepsilon_{ij}\left(10^{-8}\,C/Vm\right)$ [18].

c_{11}	c_{12}	c_{13}	c_{33}	c_{44}	c_{66}	e_{31}	e_{33}	e_{15}	ε_{11}	ε_{33}
12.6	7.91	8.39	11.7	2.30	2.35	-6.5	23.3	17.0	1.505	1.302

Table 2. The values of modulus of elasticity, density and Poisson ratio of the selected metals

Metal	E(GPa)	$\rho(kg/m^3)$	υ
Steel (St)	207	7850	0.3
Aluminum (Al)	70	2707	0.33
Magnesium (Mg)	45	1740	0.29

results confirm the reliability of the mesh sensitivity used for determining the numerical solution. Thus, for the numerical results, 6400 rectangular FEs are used in total by taking the parameters NZ=20, N=20 and M=16.

A FORTRAN code is implemented for all the programs and algorithms required for the solutions of the boundary value problems using the finite element method. The definite integrals can be evaluated numerically by Gaussian quadrature with 10 sample points. The material constants used in the numerical calculations for the piezoelectric material constituting the inclusion material are given in Table 1.

The piezoelectric inclusion(s) is/are embedded in non-piezoelectric metal materials. The mechanical constants of some of the metal materials used are given in Table 2.

It should be noted that in all numerical calculations, the polarization direction for the PZT material is taken as Ox_2. In this case, the material matrices given in Eq. (6) for the PZT material for the Ox_2 poled direction [18] are as follows:

$$\begin{Bmatrix} c_{11} & c_{13} & c_{12} & 0 & 0 & 0 \\ c_{13} & c_{33} & c_{13} & 0 & 0 & 0 \\ c_{12} & c_{13} & c_{11} & 0 & 0 & 0 \\ 0 & 0 & 0 & c_{44} & 0 & 0 \\ 0 & 0 & 0 & 0 & c_{66} & 0 \\ 0 & 0 & 0 & 0 & 0 & c_{44} \end{Bmatrix}, \begin{Bmatrix} 0 & 0 & 0 & 0 & 0 & e_{15} \\ e_{31} & e_{33} & e_{31} & 0 & 0 & 0 \\ 0 & 0 & 0 & e_{15} & 0 & 0 \end{Bmatrix}, \begin{Bmatrix} \varepsilon_{11} & 0 & 0 \\ 0 & \varepsilon_{33} & 0 \\ 0 & 0 & \varepsilon_{11} \end{Bmatrix}$$

For determination of the effect of the electro-mechanical coupling on stress distributions, numerical results are determined in two cases.

Case 1: The dielectric and piezoelectric constants of the PZT plate's material are equated to zero i.e., $e_{ij}=0,\ \varepsilon_{ij}=0$.

Case 2: The piezoelectric constants of the PZT plate materials differ from zero i.e., $e_{ij}\neq 0,\ \varepsilon_{ij}\neq 0$.

In Figure 4, the stress distribution in the rectangular thick plate made of homogeneous isotropic material $(E_2/E_1=1)$ at different $\gamma_{31}=\ell_3/\ell_1$ parameter values is examined in the cross section of $x_3=\ell_3/2,\ x_2=0$. As the value of the $\gamma_{31}=\ell_3/\ell_1$ parameter increases, the length of the plate in the direction of the specified axis increases. Accordingly, as a result of this parameter change, it will be possible to approach the limit values that can be obtained in the plane strain condition of this problem for $\gamma_{31}=\ell_3/\ell_1>1$ values. From the graphs it follows that the values of σ_{11}/p increase with $\gamma_{31}=\ell_3/\ell_1$ and converge to the value ([19]) that should be obtained in the case of plane strain. This gives us confidence of the programs and algorithms we created.

In Figure 5, the influence of the volume ratios of the single PZT inclusion in the plate (V_d/V) on the values of

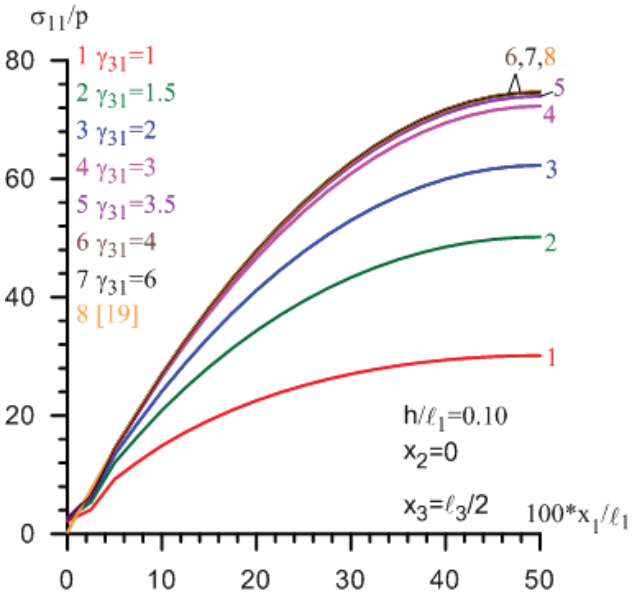

Figure 4. The effect of $\gamma_{31} = \ell_3/\ell_1$ on the values of σ_{11}/p for a homogeneous-isotropic plate under bending in the cross section of $x_3 = \ell_3/2,\ x_2 = 0$.

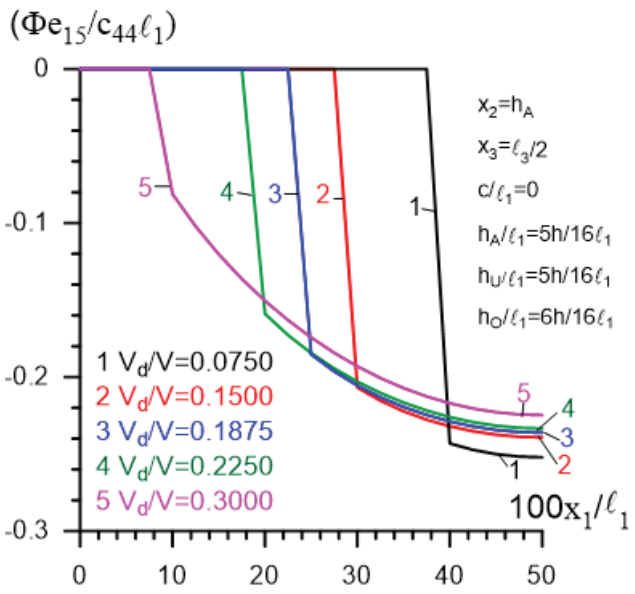

Figure 5. The effect of V_d / V on the values of $\tilde{\phi}\left(=\frac{\phi e_{15}}{c_{44}^{PZT}\ell_1}\right)$ in the cross section of $x_3 = \ell_3/2,\ x_2 = h_A$.

the electrical potential $\tilde{\phi}\left(=\frac{\phi e_{15}}{c_{44}^{PZT}\ell_1}\right)$ along the Ox_1 axis is investigated in the cross section of $x_3 = \ell_3/2,\ x_2 = h_A$. Note that V represents the total volume of the plate and V_d represents the volume of the PZT inclusion. As can be seen from the graph, as the value of the parameter V_d / V decreases, that is, as the volume fraction of the PZT inclusion in the plate decreases, the absolute values of the electrical potential increase in the considered cross section.

In Figure 6, the influence of the volume ratios (V_d / V) of the single PZT/Al inclusion for Al matrix material on the values of the differences of the stress distribution of (a) $\left((\sigma_{11})_{PZT5H}-(\sigma_{11})_{AL}\right)/p$ and (b) $\left((\tau_{12})_{PZT5H}-(\tau_{12})_{AL}\right)/p$ along the Ox_1 axis is investigated in the cross section of $x_3 = \ell_3/2,\ x_2 = h_A$ for both cases. As seen in Figure 6 (a and b), as the volume of the inclusion increases, the absolute values of (a) $\left((\sigma_{11})_{PZT5H}-(\sigma_{11})_{AL}\right)/p$ and (b) $\left((\tau_{12})_{PZT5H}-(\tau_{12})_{AL}\right)/p$ increase. In addition, as the volume of the inclusion increases, the difference between the stress

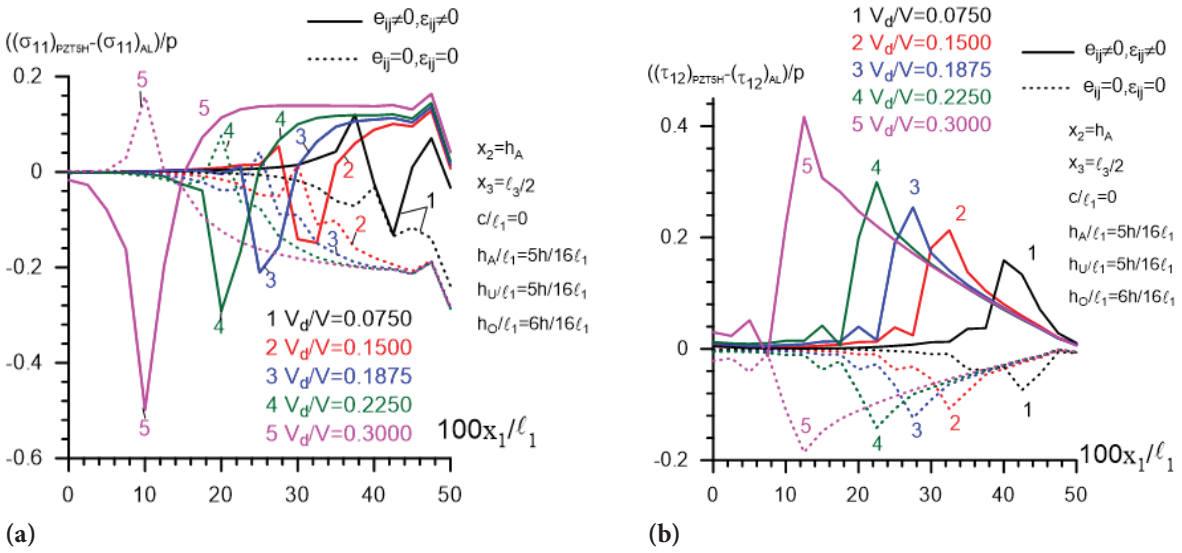

Figure 6. The effect of V_d / V on the values of (a) $\left((\sigma_{11})_{PZT5H}-(\sigma_{11})_{AL}\right)/p$; (b) $\left((\tau_{12})_{PZT5H}-(\tau_{12})_{AL}\right)/p$ in the cross section of $x_3 = \ell_3/2,\ x_2 = h_A$.

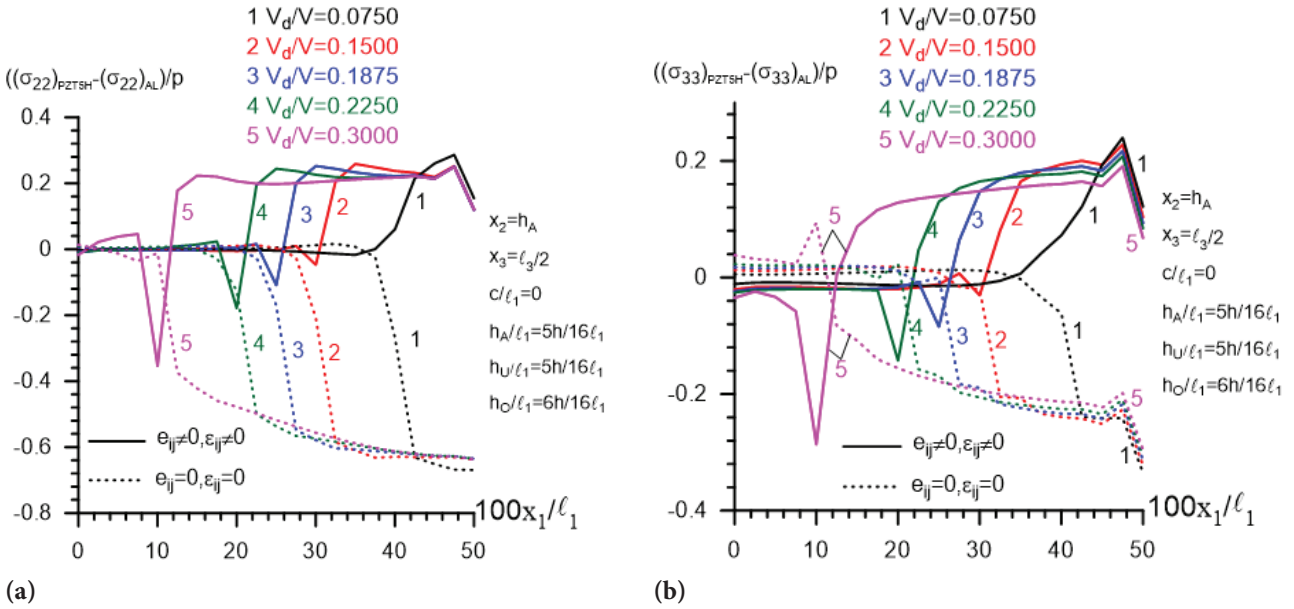

Figure 7. The effect of V_d / V on the values of (a) $\left((\sigma_{22})_{PZT5H}-(\sigma_{22})_{AL}\right)/p$; (b) $\left((\sigma_{33})_{PZT5H}-(\sigma_{33})_{AL}\right)/p$ in the cross section of $x_3 = \ell_3/2$, $x_2 = h_A$.

values obtained in Case 2 and the values obtained in Case 1 increase for $\left((\sigma_{11})_{PZT5H}-(\sigma_{11})_{AL}\right)/p$. For the values of the differences of stress distribution of $\left((\tau_{12})_{PZT5H}-(\tau_{12})_{AL}\right)/p$, $(\tau_{12})_{PZT5H} > (\tau_{12})_{AL}$ inequality is obtained for Case 2, while $(\tau_{12})_{PZT5H} < (\tau_{12})_{AL}$ inequality is obtained for Case 1.

In Figure 7, the influence of the volume ratios (V_d / V) of the single PZT/Al inclusion for Al matrix material on the values of the differences of stress distribution of (a) $\left((\sigma_{22})_{PZT5H}-(\sigma_{22})_{AL}\right)/p$ and (b) $\left((\sigma_{33})_{PZT5H}-(\sigma_{33})_{AL}\right)/p$ along the Ox_1 axis is investigated in the cross section of $x_3 = \ell_3/2$, $x_2 = h_A$ for both cases. In both graphs, the absolute values of stress differences obtained for Case 1 remain larger than the stress differences obtained for Case 2 for the cross section without edge effects. In other words, the fact that the inclusion material is PZT reduces the stress difference values. As the inclusion volume decreases, the difference values obtained for Case 1 and Case 2 increase. The presence of PZT inclusion in the plate causes an average of 40% change in stress values (Figure 6-Figure 7) at the interface between the matrix and PZT inclusion(s).

Figure 8 shows the influence of the upward replacement of the position of the PZT inclusion (i.e., reducing of the parameter h_U / ℓ_1) on the values of $\tilde{\phi}\left(=\frac{\phi e_{15}}{c_{44}^{PZT}\ell_1}\right)$ along the Ox_2 axis for PZT-5H inclusions with Ox_2 polled axis/ AL matrix for both cases in the cross section of $x_1 = \ell_1/2$, $x_3 = \ell_3/2$. From the graphs it follows that the absolute values of the electrical potential decrease with decreasing h_U / ℓ_1 along the Ox_2 axis.

Figure 9 shows the effect of the upward replacement of the position of the PZT inclusion (i.e., reducing of the parameter h_U / ℓ_1) on the values of (a) σ_{11} / p and (b) σ_{22} / p along the Ox_1 axis for PZT-5H inclusions with Ox_2 polled axis/ AL matrix for both cases in the cross section of $x_3 = \ell_3/2$, $x_2 = h_A$. From these graphs it follows that the values of the stresses of σ_{11} / p decrease with decreasing h_U / ℓ_1 for both cases, but the difference between the cases increases (Figure 9a). On the other hand, as the value of

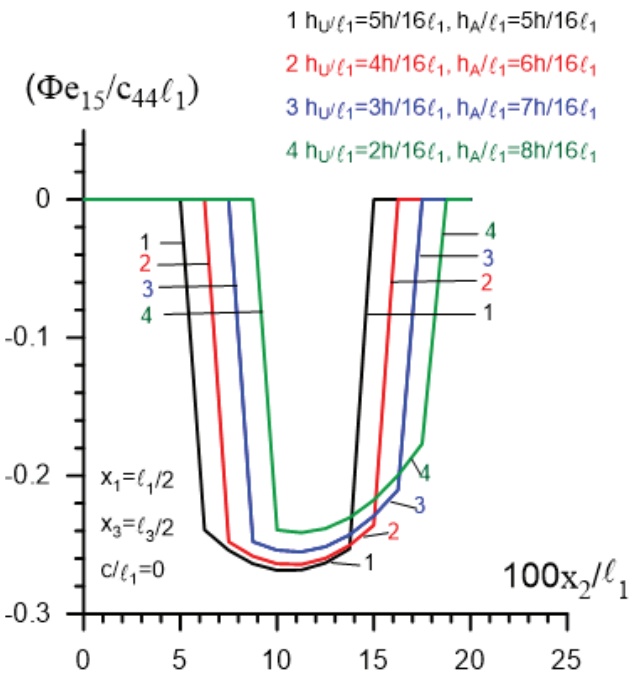

Figure 8. The effect of h_U / ℓ_1 on the values of $\tilde{\phi}\left(=\frac{\phi e_{15}}{c_{44}^{PZT}\ell_1}\right)$ for PZT-5H inclusion with Ox_2 polled axis/ AL matrix for Case 2 in the cross section of $x_1 = \ell_1/2$, $x_3 = \ell_3/2$.

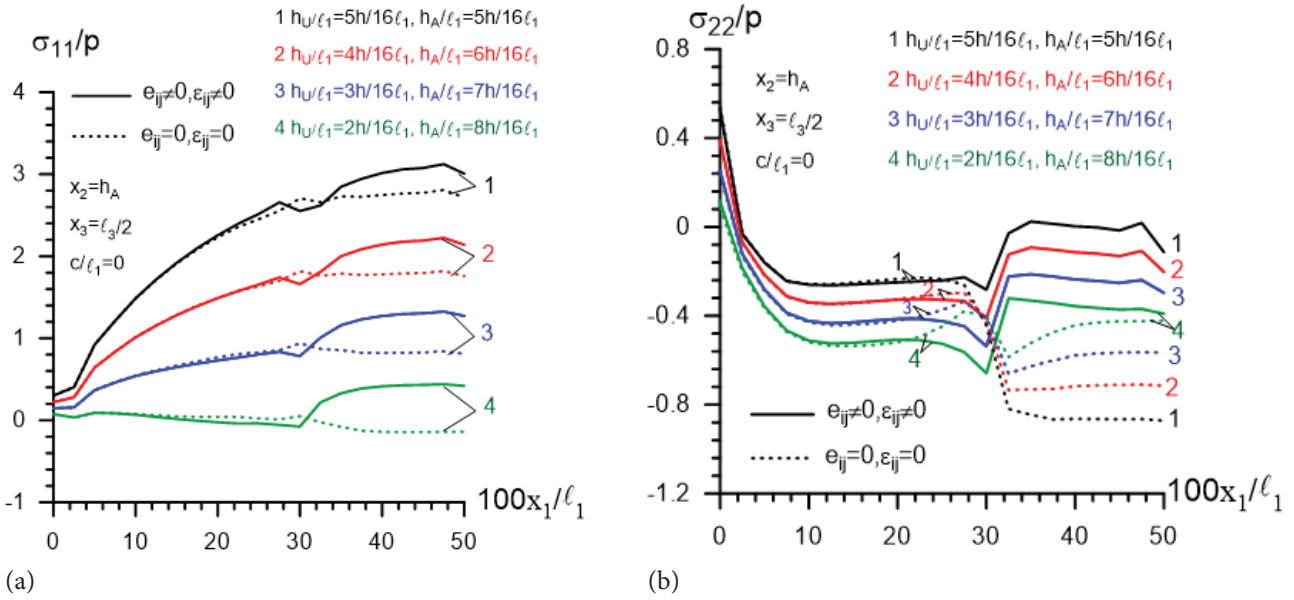

Figure 9. The effect of h_U / ℓ_1 on the values of (a) σ_{11} / p; (b) σ_{22} / p for PZT-5H inclusion with Ox_2 polled axis/ AL matrix for both cases in the cross section of $x_3 = \ell_3/2,\ x_2 = h_A$.

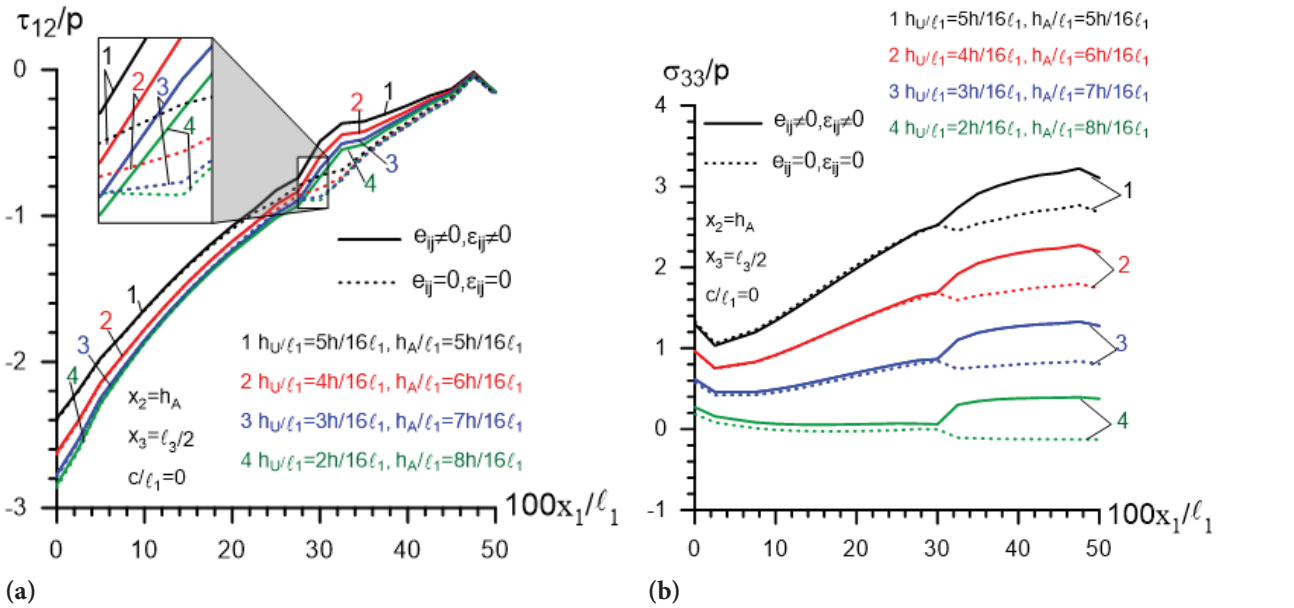

Figure 10. The effect of h_U / ℓ_1 on the values of (a) τ_{12} / p ; (b) σ_{33} / p for PZT-5H inclusion with Ox_2 polled axis/ AL matrix for both cases in the cross section of $x_3 = \ell_3/2,\ x_2 = h_A$.

the parameter h_U / ℓ_1 decreases, the absolute values of the stresses of σ_{22} / p within the boundaries of inclusion increase for Case 2, while they decrease for Case 1, and therefore the difference between these cases decreases (Figure 9b).

Figure 10 shows the effect of the upward replacement of the position of the PZT inclusion (i.e., reducing of the parameter h_U / ℓ_1) on the values of (a) τ_{12} / p and (b) σ_{33} / p along the Ox_1 axis for PZT-5H inclusions with Ox_2 polled axis/ AL matrix for both cases in the cross section of $x_3 = \ell_3/2,\ x_2 = h_A$. From the graphs it follows that the absolute values of the shear stresses of τ_{12} / p increase with decreasing h_U / ℓ_1 within the boundaries of inclusion, and the change in Case 2 is more than the change in Case 1 (Figure 10a). On the other hand, as the value of the parameter h_U / ℓ_1 decreases, the values of the stresses of σ_{33} / p within the boundaries of inclusion decrease for both cases, but the difference between these cases increases (Figure 10b).

Figure 11 indicates the values of the stresses of (a) σ_{11}/p, (b) σ_{22}/p, (c) τ_{12}/p and (d) σ_{33}/p along the Ox_1 axis for the various materials of the matrix with PZT-5H inclusion for the Ox_2 polled axis. It can be concluded that the difference between Case 1 and Case 2 is greatest for the ST matrix and smallest for the MG matrix for all stress distributions. So, the effect of piezoelectricity on the stress distributions is maximum for the ST matrix material.

Figure 12 shows the effect of the distance between the inclusions along the Ox_1 axis, i.e. the influence of the parameter c/ℓ_1 on the values of the electrical potential $\tilde{\phi}\left(=\frac{\phi e_{15}}{c_{44}^{PZT}\ell_1}\right)$ for PZT-5H inclusions with Ox_2 polled axis/ AL matrix for both cases in the cross section of $x_3 = \ell_3/2$, $x_2 = h_A$. It should be noted that as the value of the c/ℓ_1 ratio decreases, the PZT inclusions get closer to each other, and $c/\ell_1 = 0$ indicates the case where the plate contains a single inclusion (Problem 1). The total volume of the two inclusions contained in the plate in Problem 2 is equal to the volume of the single inclusion considered in Problem 1. As can be seen from the graph, as the value of the parameter c/ℓ_1 decreases, that is, as the PZT inclusions get closer to each other, the electric potential values in the considered section are affected very little.

Figure 13 shows the effect of the distance between the inclusions along the Ox_1 axis, i.e. the influence of the parameter c/ℓ_1 on the values of the stresses of (a) σ_{11}/p, (b) σ_{22}/p for PZT-5H inclusions with Ox_2 polled axis/ AL matrix for

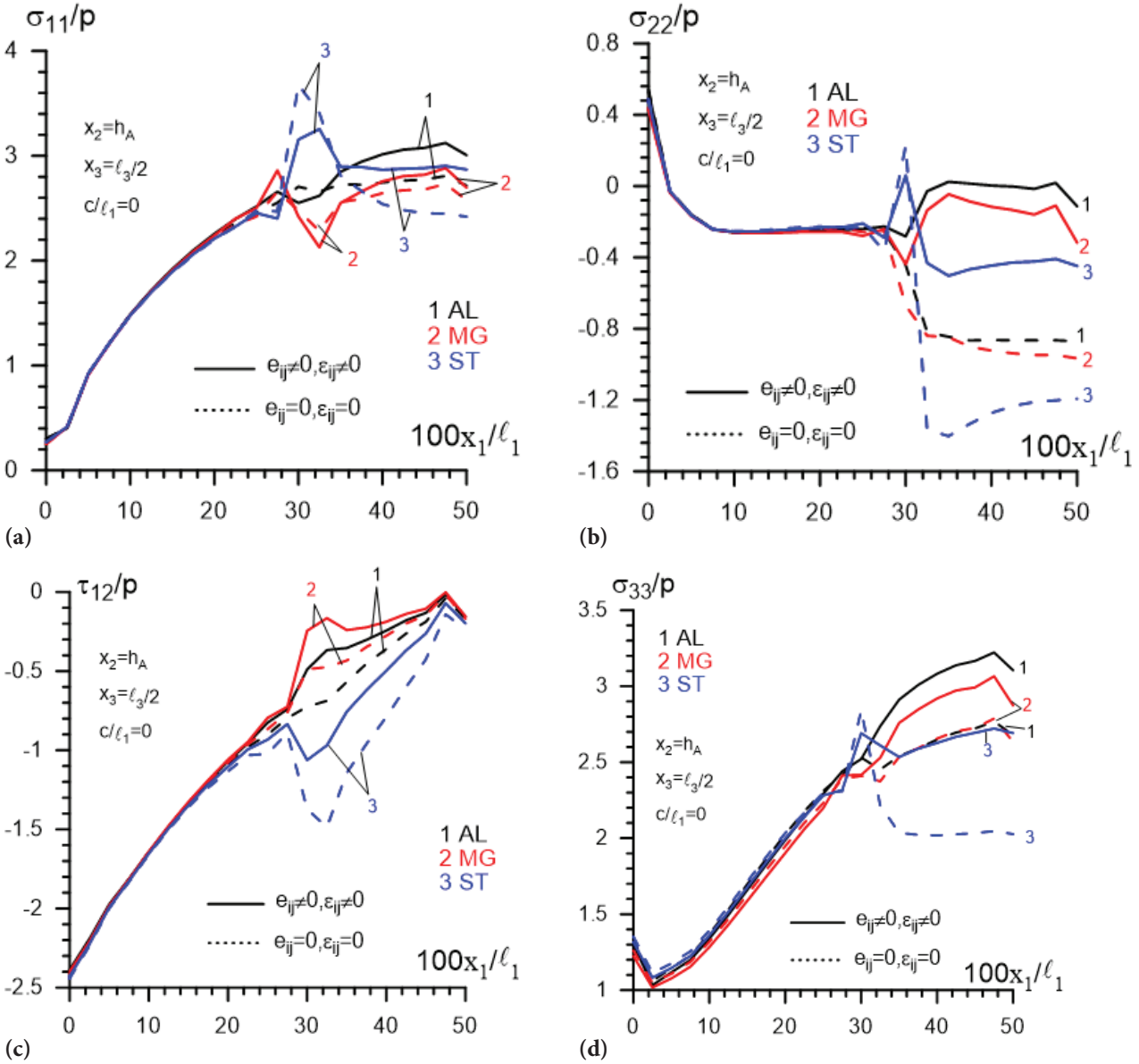

Figure 11. The effect of various matrix materials on the values of (a) σ_{11}/p, (b) σ_{22}/p, (c) τ_{12}/p and (d) σ_{33}/p for PZT-5H inclusion with Ox_2 polled axis for both cases in the cross section of $x_3 = \ell_3/2$, $x_2 = h_A$.

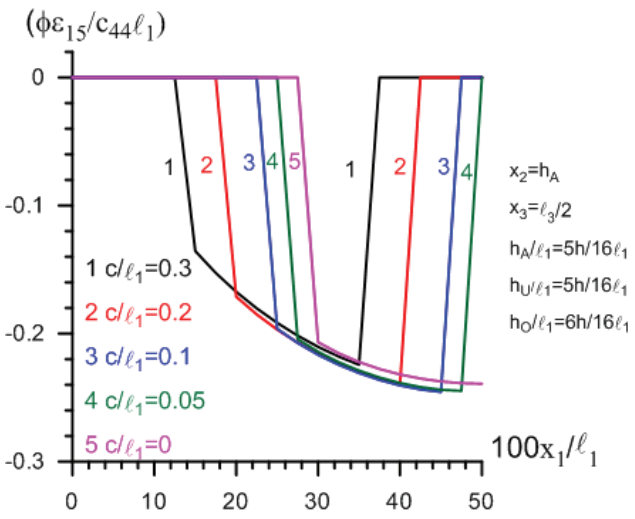

Figure 12. The effect of c/ℓ_1 on the values of $\tilde{\phi}\left(=\frac{\phi e_{15}}{c_{44}^{PZT}\ell_1}\right)$ for PZT-5H inclusions with Ox_2 polled axis/ AL matrix for both cases in the cross section of $x_3 = \ell_3/2$, $x_2 = h_A$.

CONCLUSION

In this study, the electro-static analysis of the rectangular prismatic form of the composite thick plate containing PZT inclusion(s) under the effect of bending is solved numerically with the help of the Finite Element Method, within the framework of the three-dimensional exact equations of the theory of electro-elasticity. The effects of various matrix materials, the size, volume fraction and location of the piezoelectric inclusions as well as the coupling effect between the mechanical and electrical fields on the stress distribution in the structure are investigated. Based upon the discussion in this paper, the following conclusions can be established:

- The absolute values of electrical potential decrease with the volume fraction of the PZT inclusion in the plate;
- PZT inclusion(s) within the rectangular plate under bending force causes a decrease in the values of normal stresses and causes an increase in the values of shear stresses at the interface between the matrix and PZT inclusion(s).
- The fact that the inclusion material is PZT increases the stress difference values of σ_{11}/p and τ_{12}/p; and reduces the stress difference values of σ_{22}/p and σ_{33}/p;
- As the volume of the inclusion in the structural element increases, the difference between Case 2 (considering the piezoelectric characteristics of the PZT material of inclusion) and Case 1 (considering the material inclusion as elastic) increases for σ_{11}/p and τ_{12}/p, but decreases for σ_{22}/p and σ_{33}/p;

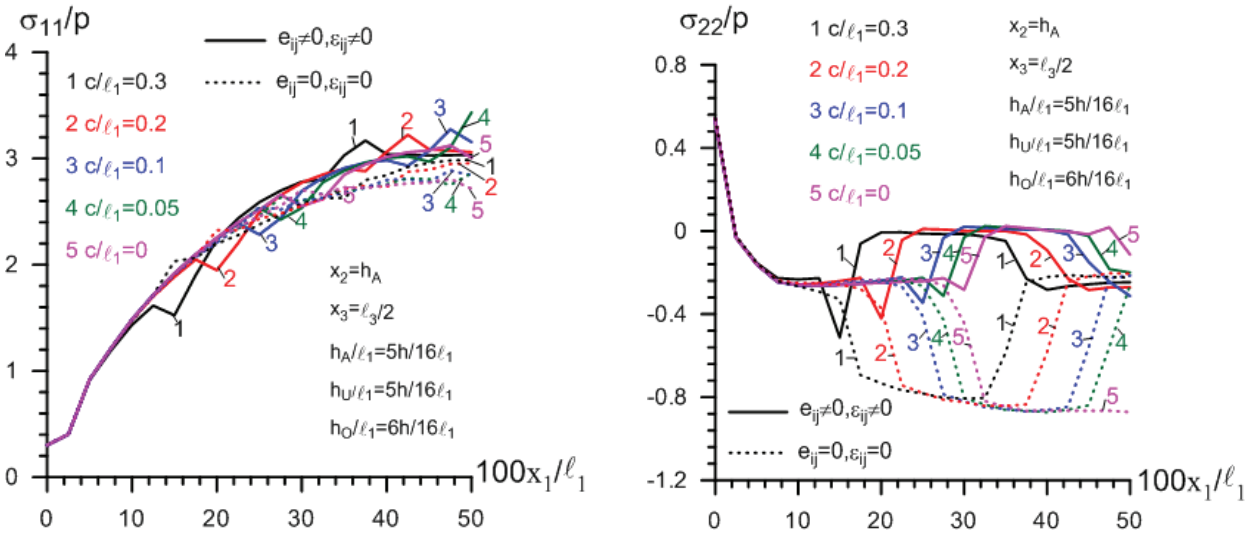

Figure 13. The effect of c/ℓ_1 on the values of (a) σ_{11}/p, (b) σ_{22}/p for PZT-5H inclusions with Ox_2 polled axis/ AL matrix for both cases in the cross section of $x_3 = \ell_3/2$, $x_2 = h_A$.

both cases in the cross section of $x_3 = \ell_3/2$, $x_2 = h_A$. When there are two parallel inclusions in the structure, the greatest change in the stress distribution is in the starting and ending sections of the inclusions. As can be seen from the graphs given in Figure 13, as the value of the parameter c/ℓ_1 decreases, that is, as the PZT inclusions get closer to each other, the places where the stress distribution changes are displaced according to the inclusions' positions, and, as the inclusions get closer to each other, the numerical values are affected very little for both stresses. The mutual effect of inclusions does not make a significant difference for elastic/ PZT inclusions.

- As the PZT inclusion approaches the upper face plane of the plate for both cases, the values of the stresses of σ_{11} / p and σ_{33} / p decrease for both cases, the absolute values of the stress of σ_{22} / p decrease for Case 1 but increase for Case 2, and the values of the stresses τ_{12} / p increase;
- The absolute values of the electrical potential decrease as the PZT inclusion approaches the upper face plane of the plate along the Ox_2 axis;
- The effect of piezoelectricity on the stress distributions is maximum for the ST matrix material;
- When there are two parallel inclusions in the structure, the greatest change in stress distribution is found in the starting and ending cross sections of the inclusions. As the PZT inclusions get closer to each other, the places where there is a change in the stress distribution are displaced according to the position of the inclusions, and, as the inclusions get closer to each other, the numerical values are slightly affected for the stresses;
- The mutual effect of inclusions does not make a significant difference for elastic/PZT inclusions.

We recall that the aim of present investigation is to provide new scientific information about the effect of a PZT inclusion(s) on the static characteristics of elastic plates. Since the exact theory is used, it is valid for both thin and thick plates and forms a reference to studies with approximate plate theory. Different geometric form of PZT inclusion(s) may be used in some future applications to decrease the stress concentrations of construction elements.

Moreover, in the present study, the mathematical modeling of the problem under consideration is given for the geometrically linear case. These investigations can be extended to the study of nonlinear problems. However, under the solution of these nonlinear problems, the finite element mesh and some parts of the FEM modeling used in the present study can also be employed.

AUTHORSHIP CONTRIBUTIONS

Authors equally contributed to this work.

DATA AVAILABILITY STATEMENT

The authors confirm that the data that supports the findings of this study are available within the article. Raw data that support the finding of this study are available from the corresponding author, upon reasonable request.

CONFLICT OF INTEREST

The author declared no potential conflicts of interest with respect to the research, authorship, and/or publication of this article.

ETHICS

There are no ethical issues with the publication of this manuscript.

REFERENCES

[1] Aksüt H. Piezoelektrik kompozitlerin elektromekanik özelliklerinin analizi. Yüksek Lisans Tezi. İstanbul: İTÜ Fen Bilimleri Enstitüsü; 2020.

[2] Wang B. Three-dimensional analysis of an ellipsoidal inclusion in a piezoelectric material. Int J Solids Struct 1992;29:293–308. [CrossRef]

[3] Fan H, Qin S A. Piezoelectric sensor embedded in a non-piezoelectric matrix. Int J Eng Sci 1995;33:379–388. [CrossRef]

[4] Xu XL, Rajapakse RKND. Boundary element analysis of piezoelectric solids with defects. Comp Part B 1998;29B:665–669. [CrossRef]

[5] Gonenli C, Das O. Effect of crack location on buckling and dynamic stability in plate frame structures. J Braz Soc Mech Sci Eng 2021;43:311. [CrossRef]

[6] Das O, Ozturk H, Gonenli C. Finite element vibration analysis of laminated composite parabolic thick plate frames. Steel and Composite Structures 2020;35:43–59.

[7] Gonenli C, Ozturk H, Das O. Effect of crack on free vibration of a pre-stressed curved plate. Proceed Inst Mech Eng C 2022;236:811–825. [CrossRef]

[8] Xiao ZM, Bai J. On piezoelectric inhomogeneity related problem-part I: a close-form solution for the stress field outside a circular piezoelectric inhomogeneity. Int J Eng Sci 1999;37:945–959. [CrossRef]

[9] Gao Y, Wang M, Zhao B. The remarkable nature of radially symmetric deformation of anisotropic piezoelectric inclusion. Acta Mech Solid Sinica 2008;21:278–282. [CrossRef]

[10] Mishra D, Park CY, Yoo SH, Pak YE. Closed-form solution for elliptical inclusion problem in antiplane piezoelectricity with far-field loading at an arbitrary angle. Eur J of Mech A/Solids 2013;40:186–197. [CrossRef]

[11] Mishra D, Yoo SH, Park CY, Pak YE. Elliptical ınclusion problem ın antiplane piezoelectricity: Stress concentrations and energy release rates. Int J Fract 2013;179:213–220. [CrossRef]

[12] Lee YT, Chen JT, Kuo SR. Null-field integral approach for the piezoelectricity problems with multiple elliptical inhomogeneties. Eng Analy with Bound Elements 2014;39:111–120. [CrossRef]

[13] Zhou ZD, Zhao SX, Kuang ZB. Stress and electric displacement analyses in piezoelectric media with an elliptic hole and a small crack. Int J Solids Struct 2005;42:2803–2822. [CrossRef]

[14] Yang BH, Gao CF. Plane problems of multiple piezoelectric inclusions in a non-piezoelectric matrix. Int J Eng Sci 2010;48:518–528. [CrossRef]

[15] Kirilyuk VS, Levchuk OI. Stress state of an orthotropic piezoelectric body with a triaxial ellipsoidal inclusion subject to tension. Int Appl Mech 2019;55:305–310. [CrossRef]

[16] Babuşcu Yeşil Ü, Yahnioğlu N, Uçan Y. Electrostatic analysis of rectangular thick plate containing piezoelectic prismatic inclusion wıth FEM. Omer Halisdemir Univ J Eng Sci 2019;8:69–81.

[17] Zienkiewicz OC, Taylor RL. The Finite Element Methods: Basic Formulation and Linear Problems. 4th ed. Oxford: Mc Graw-Hill Book Company; 1989.

[18] Yang J. An Introduction to The Theory of Piezoelectricity. New York: Springer; 2005.

[19] Yahnioğlu N. Eğrisel yapıya sahip kompozit malzemeden hazırlanmış yapı elemanlarının statiğine uygun sınırdeğer problemlerinin FEM ile incelenmesi. Doktora Tezi. İstanbul: Yıldız Teknik Üniversitesi Fen Bilimleri Enstitüsü; 1996.